ChemComm

Accepted Manuscript

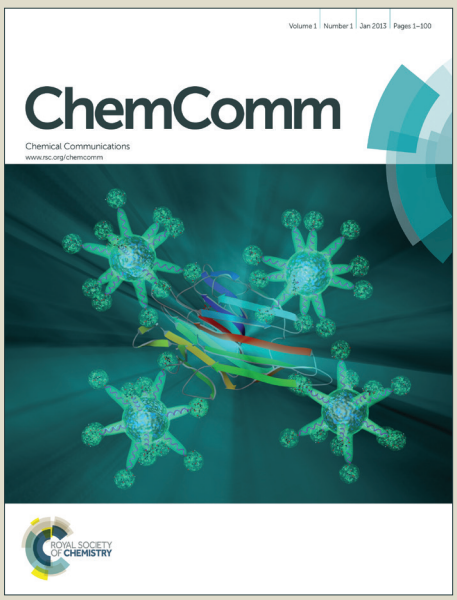

ROYAL SOCIETY OF CHEMISTRY

www.rsc.org/chemcomm

Journal Name

RSCPublishing

COMMUNICATION

Tuning Macrocycles to Design 'Turn-on' Fluorescence Probes for Manganese (II) Sensing in Live Cells

Cite this: DOI: 10.1039/x0xx00000x

Subha Bakthavatsalam†, Anindita Sarkar†, Ananya Rakshit, Shubhi Jain, Amit Kumar and Ankona Datta*

Received 00th January 2014,
Accepted 00th January 2014

DOI: 10.1039/x0xx00000x

www.rsc.org/

We tune the coordination environment of macrocyclic ligands to design two novel fluorescence sensors for Mn^{2+}. The BODIPY-based Mn^{2+} sensor M1 affords an excellent, 52 fold, fluorescence 'turn-on' response despite the paramagnetic nature of Mn^{2+}. The lipophilic probe is cell-permeable and confocal imaging demonstrates that the sensor distinctly detects Mn^{2+} within live cells.

Mn^{2+} is essential for biological systems as a cofactor for enzymes in its bound form and as an antioxidant when labile.[1-3] Mn-containing compounds also find extensive applications in industrial processes.[4] Pesticides, anti-knock agents, and infant formula contain Mn in different forms.[4] Exposure through these sources however, can lead to Mn accumulation and neuronal defects in biological systems.[4-6] The subtle balance between essentiality and toxicity is extremely intriguing, and there are many open questions related to the cellular effects of Mn^{2+} and factors maintaining homeostasis.[3, 7] A key requirement for attempts towards elucidating cellular mechanisms is obtaining information on the *in cellulo* localization of Mn^{2+} both under physiological and overexposure conditions.

Optical sensing using fluorescence is ideal for detecting trace metals because of its high sensitivity.[8] Justifiably multiple groups have reported various elegant fluorescent sensors for transition metal ions.[8-24] Mn^{2+}, however remains elusive, due to the lack of Mn-selective ligands and the paramagnetic nature of Mn^{2+} which leads to fluorescence quenching. Hence, there are only few reports on fluorescence sensors for Mn^{2+}.[25-31] We have therefore critically assessed the coordination preferences of Mn^{2+} to design Mn^{2+} specific ligands and report herein the synthesis and properties of Mn^{2+} selective 'turn-on' fluorescent sensors, manganese sensor 1 (M1) and manganese sensor 2 (M2). The BODIPY-based lipophilic sensors have visible excitation and emission profiles and display 52-fold and 28-fold fluorescence 'turn-on' response upon Mn^{2+} binding, for M1 and M2 respectively. M1 displayed higher selectivity towards Mn^{2+} sensing and was successfully applied for *in cellulo* imaging of Mn^{2+} using confocal microscopy.

Mn^{2+} lies in the bottom of the Irving-Williams series that predicts the relative stabilities of complexes formed by divalent transition metal ions.[32] Hence, designing Mn^{2+} specific ligands for sensor development proves to be extremely challenging. Canary and co-workers have reported that ligands containing mixed oxygen and nitrogen donor atoms might be suitable for Mn^{2+} binding.[29] A comprehensive body of work on Mn^{2+} complexes of penta-aza macrocycles acting as superoxide dismutase mimetics reported by Riley and co-workers and other groups indicate that Mn^{2+} ions prefer pentagonal bi-pyramidal coordination geometry.[33, 34] We therefore hypothesize that penta-aza macrocyclic motifs with oxygen containing arms can be optimized for selective Mn^{2+} sensing over other divalent metal ions (Scheme1).

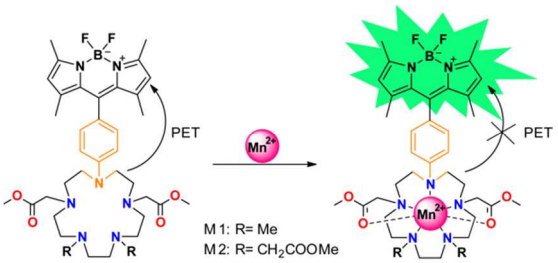

Scheme 1 Design strategy for 'turn-on' Mn^{2+} sensing.

Department of Chemical Sciences, Tata Institute of Fundamental Research, 1 Homi Bhabha Road, Colaba, Mumbai- 400005, India.

† Equal Contribution

Electronic Supplementary Information (ESI) available: Synthetic procedures, characterization, and spectra. See DOI: 10.1039/c000000x/

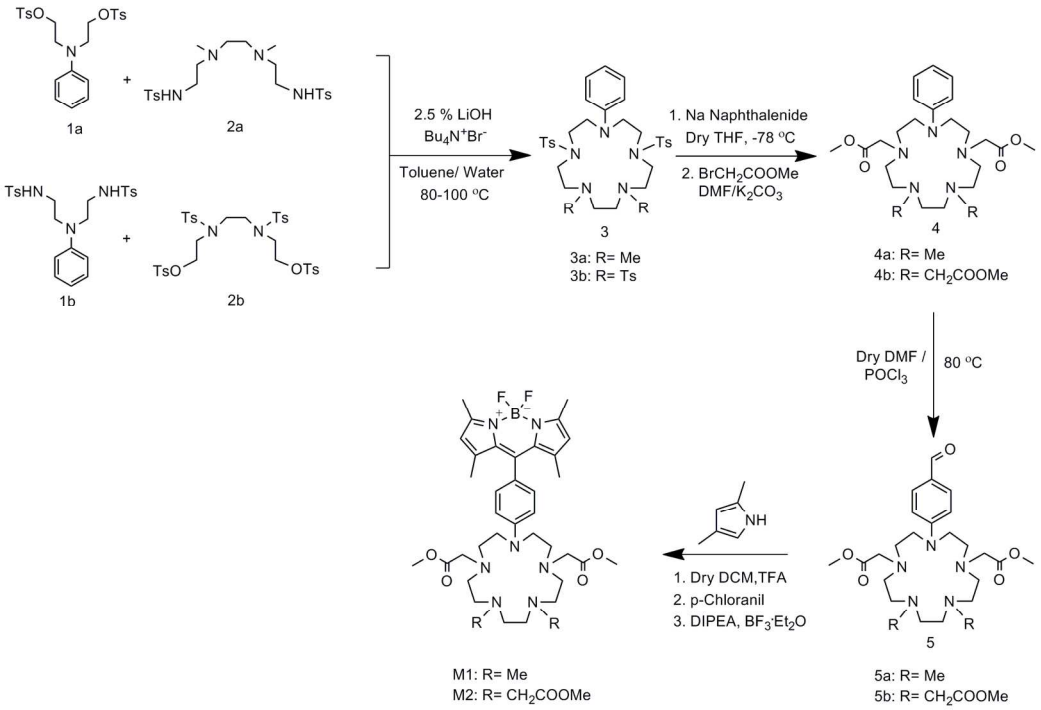

Scheme 2 Synthesis of 'turn-on' Mn^{2+} sensors.

In order to achieve efficient 'turn-on' Mn^{2+} sensing a dimethylaniline moiety is strategically fused with the ligand. The dimethylaniline moiety and the additional N-donors in the ligand will quench the fluorescence of the covalently attached BODIPY via photo-induced electron transfer (PET) mechanism in the absence of Mn^{2+}. Upon Mn^{2+} binding to the macrocycle, the fluorophore will afford an increase in fluorescence intensity (Scheme 1).

An important requirement for Mn^{2+} sensors is the selectivity for Mn^{2+} over Ca^{2+} due to the high abundance of Ca^{2+} *in cellulo*.[35] Specifically, anionic oxygen donors will increase Ca^{2+} binding. Hence, we include methyl ester groups as oxygen donors in the ligand design. The ratio of nitrogen to oxygen donor atoms is varied to design M1 and M2 with the aim of tuning Mn^{2+} affinity and selectivity.

The synthesis of M1 and M2 is outlined in Scheme 2. Richman-Atkins cyclization is used to synthesize the two novel differentially substituted *N*-tosyl-protected macrocycles **3a** and **3b** in 29 % and 47 % yields respectively, starting from compounds **1** and **2**. The synthesis of the macrocycle precursors, compounds **1** and **2** are described in the supplementary information. The macrocycles are deprotected in the presence of sodium naphthalenide following which methyl acetate arms are attached on the free secondary amines with yields of 45 % and 21 % for compounds **4a** and **4b**, respectively. Vilsmeier–Haack reaction is used to generate aldehydes **5a** in 33 % and **5b** in 31 % yields. Condensation reactions of the aldehyde-containing macrocycles **5a** and **5b** with 2,4-dimethylpyrrole, followed by treatment with $BF_3{\cdot}Et_2O$ affords M1 in 29 % yield and M2 in 14 % yield following purification.

M1 and M2 have ester arms which increase their lipophilicity. Hence, *in vitro* absorbance and fluorescence experiments to examine the 'turn-on' response of the probes were conducted in acetonitrile. Metal-unbound aka 'apo' M1 and M2 both display a single absorption maxima at 496 nm (ε = 6.9 x 10^4 M^{-1} cm^{-1} for M1 and M2, Figure S3). The emission maxima for apo M1 and M2 were at 508 and 507 nm (λ_{ex} = 480 nm), respectively (Figures 1 and S2). Upon Mn^{2+} addition neither M1 nor M2 showed any significant shifts in either the absorption (λ_{abs}=497 nm, ε = 7.1 x 10^4 M^{-1} cm^{-1} for M1 and M2, Figure S3) or emission maxima (λ_{em} = 508 nm for M1 and M2, Figures 1 and S2).

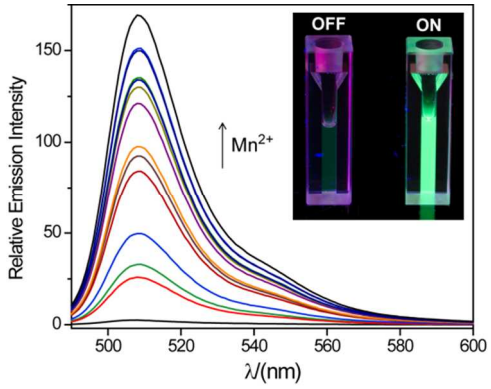

Figure 1 Fluorescence response of M1 (2.5 μM) to Mn^{2+} (0 - 48 μM) in acetonitrile. λ_{ex} = 480 nm. (inset) Image depicting quartz cuvettes containing M1 (10 μM, left) and M1 (10 μM) in presence of Mn^{2+} (20 μM, right). Both cuvettes were illuminated equally under long-wave UV radiation (λ_{ex} = 365 nm).

Both M1 and M2 displayed excellent fluorescence 'turn-on' response in the presence of Mn^{2+}. The apo forms of M1 and M2 had very low quantum yields (ϕ = 0.0038 for M1 and 0.0055

for M2) due to effective quenching of the BODIPY fluorophore via the dimethylaniline moiety fused to the penta-aza macrocycle (Figures 1 and S2). Upon addition of Mn^{2+}, M1 afforded a 52 fold emission enhancement (ϕ = 0.197, Figure 1 and 1 inset), while M2 afforded a 28 fold emission enhancement ((ϕ = 0.156, Figure S2).

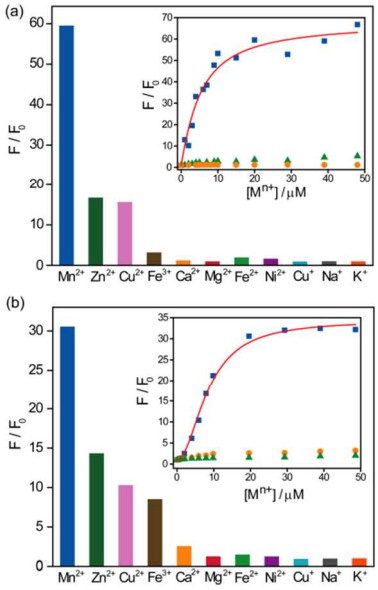

Figure 2 Observed fluorescence intensity (F) over initial fluorescence intensity in the absence of any metal ion (F_0) for (a) M1 (2.5 μM) and (b) M2 (2.5 μM) in the presence of various biologically relevant metal ions ([M^{n+}]= 20 μM) at 508 nm, in acetonitrile. λ_{ex} = 480 nm. Insets: F/F_0 at 508 nm for (a) M1 and (b) M2 in the presence of Mn^{2+} (blue squares, fitted data red line), Ca^{2+} (orange circles), and Fe^{2+} (green triangles) over a [M^{n+}] range (0-48 μM).

The fluorescence binding plots (Figures 2a inset and 2b inset) were fitted to obtain apparent dissociation constants for Mn^{2+} binding to M1 and M2 in acetonitrile, which were 4.0 ± 0.9 μM and 8.3 ± 0.4 μM respectively. The plot for M1 could be best fitted to a 1:1 binding model (Equation S1) with no cooperativity as indicated by the corresponding Hill plot (Figure S4a). On the other hand, the binding plot for M2 was best fitted to a 1:2 (M2:Mn^{2+}) binding model (Equation S2). A Hill plot in this case displayed cooperative binding (Figure S4b), hinting at a possible second Mn^{2+} binding site due to the presence of additional methyl acetate arms.

We probed the selectivity of M1 and M2 towards other biologically relevant metal ions by performing fluorescence titration experiments. F/F_0 values for the probes at the emission maxima, 508 nm, have been plotted for various metal ions in Figures 2a and 2b. Amongst the ions tested, both M1 and M2 afforded maximum fluorescence enhancement in the presence of Mn^{2+} and the fluorescence response saturated above 20 μM Mn^{2+} concentration (Figures 2a inset and 2b inset). Importantly, Ca^{2+}, a major competitor for Mn^{2+} binding ligands, did not display any fluorescence enhancement with M1(Figures 2a and 2a inset) and only a modest 2.6 times increase with M2 (Figures 2b and 2b inset). Similarly, another paramagnetic metal ion Fe^{2+} did not afford any increase in emission in the presence of either sensor (Figures 2a and 2b).

M1 afforded better selectivity towards Mn^{2+} when compared to M2. The only other biologically relevant metal ions that afforded a response with M1 were Zn^{2+} and Cu^{2+} (Figure 2a). Since, intracellular Cu is mostly present as Cu^{+} in the reducing intracellular environment, interference from Cu^{2+} during *in cellulo* Mn^{2+} imaging is not expected.[21] Also, intracellular labile Zn^{2+} is in the pM level, while the putative labile Mn^{2+} is predicted to be in the sub μM level.[35-37] Competition experiments performed by adding Mn^{2+} following additions of Zn^{2+} or Cu^{2+} to either probe indicated further increase in fluorescence emission (Figure S5). Hence, M1 and M2 respond to Mn^{2+} even in the presence of these interfering ions, proving higher Mn^{2+} specificity. Another metal ion that responded to the sensors was Cd^{2+} (Figure S6). However Cd^{2+} is highly toxic to cells and is not generally present in labile form.[35] Hence, we do not expect any interference due to this ion in the cellular milieu.

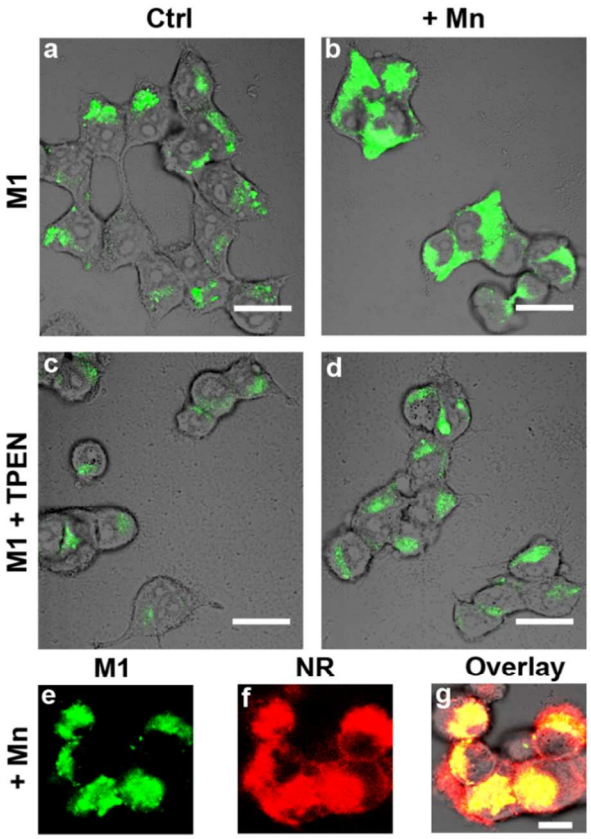

Figure 3 Live-cell imaging of intracellular Mn^{2+} by confocal microscopy in HEK 293T cells. Overlay of confocal and transmission images of cells treated with (a) M1 (b) $MnCl_2$ (25 μM) in growth media followed by M1 (c) M1 followed by TPEN (2mM) (d) $MnCl_2$ followed by M1 and TPEN. λ_{ex} 488 nm (e-g) Confocal images depicting co-localization of M1 (green channel, λ_{ex} 488 nm) with Nile Red (100 nM, red channel, λ_{ex} 543 nm) in Mn-treated cells. M1 concentration 5 μM. Scale: 25 μm (a-d), 10 μm (e-g).

The probes are lipophilic and hence would be applicable for *in cellulo* imaging of Mn^{2+} in lipid-rich bodies and organelles.

In order to test the *in cellulo* response we chose M1 since it had higher selectivity for Mn^{2+}. M1 was dissolved in DMSO and diluted in Thomson's buffer (< 1 % DMSO in buffer, pH 7.4) for the cell experiments. All experiments and imaging were performed on live HEK 293T cells. The probe readily entered cells within 15 min of incubation, as shown in the confocal images in figure 3. Cells treated with $MnCl_2$ for 1h showed significant fluorescence enhancement when compared to control untreated cells (Figures 3 a, b). To test whether the fluorescence increase was due to Mn^{2+}, tetrakis-(2-pyridylmethyl)ethylene-diamine (TPEN) a cell-permeable chelator of divalent metal ions was added to the Mn-treated cells. The emission intensity clearly decreased (Figure 3d) proving that the increase in emission intensity was a Mn^{2+} selective response. The fluorescence intensity in control cells also decreased upon TPEN treatment indicating that the sensor would also be able to detect labile Mn^{2+} under physiological conditions (Figures 3c).

Finally, to check the *in cellulo* localization of the sensors we performed co-localization experiments with Nile Red, a cell-permeable lipophilic dye known to bind to lipid membranes.[38] The confocal images indicate that M1 co-localizes with Nile Red (Figure 3e-g), implying that the sensor targets lipid vesicles and senses Mn^{2+} in cellular bodies with high lipid-content.

In this work we have successfully shown that penta-aza macrocycles can be optimally decorated with oxygen containing arms to develop selective 'turn-on' fluorescent sensors for Mn^{2+}. The sensor M1 shows significant increase in fluorescence intensity in Mn^{2+}-loaded cells and can detect Mn^{2+} within lipid rich entities. Selective detection of Mn^{2+} is distinctly confirmed by reduction in intensity upon TPEN treatment in Mn^{2+}-treated cells. Recent micro-SXRF and XANES studies on Mn^{2+} localization within the cell indicate Mn^{2+} accumulation in the Golgi apparatus with possible removal of excess Mn^{2+} via exocytosis through lipid vesicles.[39] In the future we plan to use our modular synthetic strategy of attaching arms to penta-aza macrocycles to modify and target our sensors to the Golgi, a major site implicated in Mn^{2+} homeostasis.[40]

A.D. acknowledges support from Department of Atomic Energy, India, The authors acknowledge Prof. Sudipta Maiti and the Biophotonics group, TIFR, for help with cell culture and confocal imaging; NMR Facility, TIFR, India; and Mass laboratory, Chemistry Department, I.I.T. Bombay, India.

Notes and references

1 K. Barnese, E. B. Gralla, J. S. Valentine and D. E. Cabelli, *Proc. Natl. Acad. Sci. U.S.A.*, 2012, **109**, 6892-6897.
2 R. L. McNaughton, A. R. Reddi, M. H. S. Clement, A. Sharma, K. Barnese, L. Rosenfeld, E. B. Gralla, J. S. Valentine, V. C. Culotta and B. M. Hoffman, *Proc. Natl. Acad. Sci. U.S.A.*, 2010, **107**, 15335-15339.
3 A. R. Reddi, L. T. Jensen and V. C. Culotta, *Chem. Rev.*, 2009, **109**, 4722-4732.
4 A. B. Bowman, G. F. Kwakye, E. H. Hernandez and M. Aschner, *J. Trace Elem. Med. Biol.*, 2011, **25**, 191-203.
5 J. Kaiser, *Science*, 2003, **300**, 926-928.
6 S. Bakthavatsalam, S. Das Sharma, M. Sonawane, V. Thirumalai and A. Datta, *Dis Model Mech.*, 2014, **7**, 1239-1251.
7 C. E. Blaby-Haas and S. S. Merchant, *J. Biol. Chem.*, 2014, **289**, 28129-28136.
8 K. P. Carter, A. M. Young and A. E. Palmer, *Chem. Rev.*, 2014, **114**, 4564-4601.
9 E. M. Nolan and S. J. Lippard, *Acc. Chem. Res.*, 2009, **42**, 193-203.
10 Y. Xu, L. Xiao, S. Sun, Z. Pei, Y. Pei and Y. Pang, *Chem. Commun.*, 2014, **50**, 7514-7516.
11 S. Pal, N. Chatterjee and P. K. Bharadwaj, *RSC Adv.*, 2014, **4**, 26585-26620.
12 M. Li, H. Ge, R. L. Arrowsmith, V. Mirabello, S. W. Botchway, W. Zhu, S. I. Pascu and T. D. James, *Chem. Commun*, 2014, **50**, 11806-11809.
13 Y. H. Lee, N. Park, Y. B. Park, Y. J. Hwang, C. Kang and J. S. Kim, *Chem. Commun.*, 2014, **50**, 3197-3200.
14 M. L. Giuffrida, E. Rizzarelli, G. A. Tomaselli, C. Satriano and G. Trusso Sfrazzetto, *Chem. Commun.* , 2014, **50**, 9835-9838.
15 A. Balamurugan, V. Kumar and M. Jayakannan, *Chem. Commun.*, 2014, **50**, 842-845.
16 C. J. Fahrni, *Curr. Opin. Chem. Biol.*, 2013, **17**, 656-662.
17 Y. Chen, C. Zhu, J. Cen, J. Li, W. He, Y. Jiao and Z. Guo, *Chem. Commun.*, 2013, **49**, 7632-7634.
18 Z. Xu, X. Liu, J. Pan and D. R. Spring, *Chem. Commun.*, 2012, **48**, 4764-4766.
19 A. M. Kim, S. Vogt, T. V. O'Halloran and T. K. Woodruff, *Nat. Chem. Biol.*, 2010, **6**, 674-681.
20 Y. You, E. Tomat, K. Hwang, T. Atanasijevic, W. Nam, A. P. Jasanoff and S. J. Lippard, *Chem. Commun.*, 2010, **46**, 4139-4141.
21 E. L. Que, D. W. Domaille and C. J. Chang, *Chem. Rev.*, 2008, **108**, 1517-1549.
22 J. Liu and Y. Lu, *J. Am. Chem. Soc.*, 2007, **129**, 9838-9839.
23 J. L. Bricks, A. Kovalchuk, C. Trieflinger, M. Nofz, M. Buschel, A. I. Tolmachev, J. Daub and K. Rurack, *J. Am. Chem. Soc.*, 2005, **127**, 13522-13529.
24 M. D. Shults, D. A. Pearce and B. Imperiali, *J. Am. Chem. Soc.*, 2003, **125**, 10591-10597.
25 X. Mao, H. Su, D. Tian, H. Li and R. Yang, *ACS Appl. Mater. Interfaces*, 2013, **5**, 592-597.
26 K. Dutta, R. C. Deka and D. K. Das, *J. Fluorescence*, 2013, **23**, 1173-1178.
27 F. Gruppi, J. Liang, B. B. Bartelle, M. Royzen, D. H. Turnbull and J. W. Canary, *Chem. Commun.* , 2012, **48**, 10778-10780.
28 I. Kaya, M. Yildirim and M. Kamaci, *Synth. Met.*, 2011, **161**, 2036-2040.
29 J. Liang and J. W. Canary, *Angew. Chem. Int. Ed.*, 2010, **49**, 7710-7713.
30 Y. J. Lee, C. Lim, H. Suh, E. J. Song and C. Kim, *Sens. Actuators, B*, 2014, **201**, 535-544.
31 B. R. Jali, K. Masud and J. B. Baruah, *Polyhedron*, 2013, **51**, 75-81.
32 H. Irving and R. J. P. Williams, *J. Am. Chem. Soc.*, 1953, 3192-3210.
33 D. Lieb, I. Kenkell, J. L. Miljkovic, D. Moldenhauer, N. Weber, M. R. Filipovic, F. Groehn and I. Ivanovic-Burmazovic, *Inorg. Chem.*, 2014, **53**, 1009-1020.
34 D. Salvemini, D. P. Riley and S. Cuzzocrea, *Nat. Rev. Drug Discov.*, 2002, **1**, 367-374.
35 L. A. Ba, M. Doering, T. Burkholz and C. Jacob, *Metallomics*, 2009, **1**, 292-311.
36 R. A. Bozym, R. B. Thompson, A. K. Stoddard and C. A. Fierke, *ACS Chem. Biol.*, 2006, **1**, 103-111.
37 C. E. Outten and T. V. O'Halloran, *Science*, 2001, **292**, 2488-2492.
38 P. Greenspan, E. P. Mayer and S. D. Fowler, *J. Cell Biol.*, 1985, **100**, 965-973.
39 A. Carmona, S. Roudeau, L. Perrin, G. Veronesi and R. Ortega, *Metallomics*, 2014, **6**, 822-832.
40 S. Mukhopadhyay and A. D. Linstedt, *Proc. Natl. Acad. Sci. U.S.A.*, 2011, **108**, 858-863.

